Applied and
Computational
Mathematics
Division

NISTIR 4482

Center for Computing and Applied Mathematics

Space Marching Difference Schemes in the Nonlinear Inverse Heat Conduction Problem

Alfred S. Carasso

November 1990

SPACE MARCHING DIFFERENCE SCHEMES IN THE NONLINEAR INVERSE HEAT CONDUCTION PROBLEM

Alfred S. Carasso

U.S. DEPARTMENT OF COMMERCE
National Institute of Standards
and Technology
Applied and Computational
Mathematics Division
Center for Computing and
Applied Mathematics
Gaithersburg, MD 20899

November 1990

Space marching difference schemes in the nonlinear

inverse heat conduction problem

Alfred S. Carasso

Center for Computing and Applied Mathematics

National Institute of Standards and Technology

Gaithersburg, MD 20899

November 21, 1990

Abstract

The Lax-Ricthmyer theory is used to study the error amplification
properties of 18 space marching finite difference schemes, for the 1-D
nonlinear inverse heat conduction problem. A non-dimensional param-
eter Ω, involving the time step Δt, the effective thermal diffusivity α,
and the distance l from the sensor to the active surface, is found to
provide a measure of the numerical difficulty of the inverse calcula-
tion. All 18 schemes are unstable and blow-up like $10^{\lambda\Omega}$, where the
constant λ depends on the particular numerical method. There are
substantial differences in the λ's however, and some newly constructed
algorithms, employing forward time differences at non-adjacent mesh
points, are shown to produce relatively low values of λ. Using synthetic
noisy data, a nonlinear reconstruction problem is considered for which
$\Omega = 25$. This problem simulates heat transfer in gun barrels when a
shell is fired. It is shown that while most of the 18 schemes cannot
recover the thermal pulses at the gun tube wall, two of the new meth-
ods provide reasonably accurate results. A tendency to underestimate
peak values in fast, narrow thermal pulses is also noted.

Key Words: nonlinear heat flow, marching difference schemes, er-
ror amplification, numerical experiments.

AMS (MOS) subject classifications: 35R25, 65M30.

1 Introduction

The inverse heat conduction problem, (IHCP), whereby surface temperature and gradient histories are calculated from histories measured at an accessible interior location, remains a basic problem in many areas of heat transfer. On page 2 of the monograph by Beck, Blackwell, and St. Clair, [1], the authors indicate a variety of applications, and they estimate that some 300 papers have been written in this general area as of 1985. A substantial mathematical literature has also developed around the IHCP during the last 30 years or so, as may be seen from the bibliography in Hào and Gorenflo, [6]. An interesting new approach based on systems theory, together with a brief overview of current methods and some further references, may be found in Marquardt and Auracher, [9].

The present paper focuses exclusively on space marching finite difference methods for the one dimensional problem in a medium with temperature-dependent thermal properties. Several such methods are presented in Beck *et al*, [1]. Here, we do not discuss procedures based on replacing the heat conduction equation with an approximating hyperbolic equation, [5], [17], nor methods combining space marching with time marching, [11]. Using the Lax-Ricthmyer theory, [12], [13], we examine the l^2 norms of discrete

3

solution operators associated with several marching schemes, in the Fourier transform domain. This enables us to demonstrate the considerable differences which exist between various methods with regard to error amplification, and leads us to construct some new schemes that are relatively well-behaved. Numerical reconstruction experiments with synthetic noisy data are then used to illustrate the capabilities of the new schemes. By comparing with known 'exact' solutions, we demonstrate credible approximate solutions at parameter values that are not tractable by more standard marching algorithms.

It develops that the role of time differencing is paramount, typically overshadowing the influence of space differencing, that some $O(\Delta t)$ methods are preferable to some $O(\Delta t^2)$ methods, and that a certain kind of $O(\Delta t)$ forward time differencing can dramatically reduce error amplification. The beneficial aspects of using *future temperatures* have been noted many times in the literature. However, we provide some quantitative facts that are independent of the particular surface profiles to be reconstructed, but pertain to the schemes themselves. Computational exploration of the characteristics of 18 different methods, albeit in limited ranges of parameter values, indicates the following. In these methods, the maximum amplification factor behaves roughly according to $A_{max} \approx 10^{\lambda\Omega}$, where $\Omega = l(\alpha\Delta t)^{-1/2}$, l being the dis-

4

tance between the internal sensor and the active surface, and α the effective thermal diffusivity. The non dimensional quantity Ω reflects the underlying physical situation, including the desired resolution Δt, and provides a measure of the difficulty of the particular IHCP; Ω has the same value in each marching scheme. On the other hand, λ depends primarily on the time differencing option associated with a particular method and is essentially independent of the physical parameters and mesh sizes. We show that some forms of forward differencing are more effective than others in producing lower values for λ, while one particular future temperature method leads to a larger λ and makes things *worse*.

Marching difference schemes have been a mainstay in the numerical computation of *well-posed* initial value problems. In many cases, difficult nonlinear problems can be solved effectively by taking sufficiently small marching steps while lagging the nonlinearity at the previous step. A Courant condition, linking the sizes of the space and time increments, may need to be obeyed to maintain computational stability. However, for *ill-posed* initial value problems such as the IHCP, *all* consistent marching difference schemes are necessarily *unconditionally unstable*. In that case, no Courant condition exists that can prevent drastic error amplification if the mesh is made sufficiently fine, [12, p. 59]. The salient observation of the present

5

paper is that such marching algorithms can 'blow-up' at widely different rates as Δt, $\Delta x \downarrow 0$. Given a fixed fine mesh, error amplification may be totally overwhelming in some methods, while being sufficiently mild in other methods to permit reasonably accurate answers.

Our frame of reference for these comparisons is an artificial but representative problem with units. The object is to estimate temperature and flux histories on the surface of an SAE 4340 steel plate, using measurements from an internal sensor located 0.50 mm away from the active surface, in the presence of 0.1% added noise. The effective thermal diffusivity is on the order of 0.004 mm^2 $millisec^{-1}$, while the surface histories are pulse waveforms with a rise time of 10 $millisec$ or less. To accommodate possibly rapid changes, 1000 equispaced mesh points are placed on the time interval $0 \leq t \leq 100$ $millisec$. ($\Omega \approx 25$ in the present case). This choice of process parameters and time scales is motivated by an interesting physical problem involving nonlinear inverse heat transfer in gun barrels, and the pulse waveforms at the plate surface are chosen to simulate thermal histories at the inside wall of a cannon when a shell is fired. [4], [16]. Reconstruction of such wall histories is important in the study of gun tube erosion, [2]. Here, fabricated surface temperature histories, together with thermal diffusivity data for SAE 4340 steel, are used to create *synthetic* histories at the sensor loca-

6

tion by numerically solving a direct nonlinear heat flow problem. Uniformly distributed random noise is then added to these data, and the performance of various marching procedures is evaluated on this data set.

2 The direct nonlinear problem

The synthetic data are generated as follows. With $\omega(u) \equiv \rho(u)\, c_p(u)$ the density-specific heat product, $k(u)$ the thermal conductivity, $\alpha(u) = k(u)/\omega(u)$ the thermal diffusivity, and $f(t) = 300(1 + 0.02t - 0.12 \times 10^{-3}t^2)$, consider the following direct problem for the heat conduction equation:

$$\omega(u)\, u_t = \{k(u)\, u_x\}_x, \qquad 0 < x < 1mm, \quad 0 < t < 100millisec,$$

$$u(x,0) = 300^\circ K, \qquad 0 \le x \le 1mm,$$

$$u(1,t) = \{f(t) + 3500e^{-0.15t}sin(\pi t/40)\}^\circ K, \; 0 \le t \le 100millisec,$$

$$u(0,t) = \{300 + 250sin(\pi t/100)\}^\circ K, \qquad 0 \le t \le 100millisec. \quad (1)$$

The boundary $x = 1$ is the active surface, and $u(1,t)$ is pulse shaped, increasing from $300^\circ K$ to near $1000^\circ K$ during the first ten or so milliseconds. See Fig. 1. A boundary condition at $x = 0$ is imposed in order to close the system. (The choice for $u(0,t)$ is artificial and does not reflect any particular physical process). We assume a constant ω in the present hypothetical experiment, although nonlinearity in ω poses no additional difficulties and

7

is provided for in the marching schemes of Section 3. On dividing both sides of the heat equation by ω, $k(u)$ is replaced by $\alpha(u)$ on the right hand side. Using thermophysical data for SAE 4340 steel, [14], [15, p. 395], we postulate the following linear approximation for $\alpha(u)$ in gun tubes:

$$\alpha(u) = \{0.01 - 8.0 \times 10^{-6}(u - 250)\} \quad mm^2 \quad millisec^{-1}, \tag{2}$$

in the range $300^o K \leq u \leq 1000^o K$. In that range, $\alpha(u)$ undergoes a 240% change. Numerical computation of this direct problem was accomplished using PDECOL, [8]. This software package uses piecewise polynomial collocation methods for spatial discretization, together with adaptive step selection for marching the solution forward in time. Note that since both boundary temperatures are prescribed in (1), the boundary fluxes must be determined by solving the direct problem. In fact, temperature and flux histories at 1000 equispaced mesh points on the time interval $0 \leq t \leq T_{max} = 100 millisec$, were obtained at several interior locations x_i, as well as at the two boundaries $x = 0$ and $x = 1$. (Data at $x = 0$, 0.5, and 1, are shown in Fig. 1). Each interior data value $h(t_k)$ was then perturbed, by adding to it a random number drawn from a uniform distribution in the range $\pm 0.001h(t_k)$. In the inverse problem calculation, interior data at any one such x_i may be used as initial values in space marching schemes for reconstructing surface

8

histories. (Some schemes use $u(x_i, t)$ and $u(x_i - \Delta x, t)$, rather than $u(x_i, t)$ and $u_x(x_i, t)$). In a practical setting, temperature histories at *two* internal locations x_1, x_2, may be used to obtain temperature or flux histories at any intermediate points y, $x_1 < y < x_2$, by numerically solving the direct problem on $x_1 \leq x \leq x_2$.

3 Marching schemes and the inverse problem

Let u_j^n denote $u(j \Delta x, n \Delta t)$, where Δx, Δt are constant space and time increments, and let $\sigma_j^n = ((\Delta x)^2 \omega(u_j^n))/(\Delta t\, k(u_j^n))$, $\beta_j^n = k'(u_j^n)/k(u_j^n)$. We formulate 18 possible explicit schemes, marching in the positive x direction, for obtaining $u(1, t)$ and $u_x(1, t)$. The steady state conditions $u(x, 0) = Constant$, $u_x(x, 0) \equiv 0$, are used throughout. For schemes involving future temperatures, the duration of the sensor record, $T_{max} = N \Delta t$, is assumed sufficient to permit reconstruction of the surface waveform on a prescribed, physically relevant time interval, $T_0 = m \Delta t$, $m < N$. For such schemes, it is sometimes expedient to obtain solution values at or near T_{max}, by simple extrapolation of immediately preceding values. This procedure typically induces violent spurious oscillations in the vicinity of T_{max}. In our numerical experiments, provided the scheme was otherwise well-behaved, such end-

point artifacts did not extend beyond 5 $millisec$ to the left of T_{max}, and they did not affect reconstruction of the surface history on the remainder of the interval. Generally, the alternative of using backward difference formulae near T_{max}, as in method **S5** below, did not prevent such end-point instabilities. The first three schemes below are nonlinear generalizations of methods presented in [1, Chapter 6].

The first method, due to D'Souza, is based on implicit time differencing for the direct problem:

$$\omega(u_j^n)(u_j^n - u_j^{n-1})/\Delta t = k(u_j^n)(u_{j+1}^n - 2u_j^n + u_{j-1}^n)/(\Delta x)^2$$

$$+ \ k'(u_j^n)(u_j^n - u_{j-1}^n)^2/(\Delta x)^2 \tag{3}$$

Let $v_j^n = u_{j-1}^n$. Solving for u_{j+1}^n, we may reformulate (3) as a coupled first order space marching system involving only the nodes j, $j + 1$.

S1   D'Souza 1.

$$u_{j+1}^n = (2 + \sigma_j^n)u_j^n - \sigma_j^n u_j^{n-1} - v_j^n - \beta_j^n(u_j^n - v_j^n)^2$$

$$v_{j+1}^n = u_j^n, \qquad n = 1, \ldots, N,$$

$$u_{j+1}^0 = u_j^0, \qquad v_{j+1}^0 = v_j^0. \tag{4}$$

Explicit time differencing may also be used and leads to:

10

S2   D'Souza 2.

$$u_{j+1}^n = (2 - \sigma_j^n)u_j^n + \sigma_j^n u_j^{n+1} - v_j^n - \beta_j^n(u_j^n - v_j^n)^2$$

$$v_{j+1}^n = u_j^n, \qquad n = 1, \ldots, N - 1,$$

$$u_{j+1}^N = 2u_{j+1}^{N-1} - u_{j+1}^{N-2}$$

$$v_{j+1}^N = 2v_{j+1}^{N-1} - v_{j+1}^{N-2}$$

$$u_{j+1}^0 = u_j^0, \qquad v_{j+1}^0 = v_j^0. \tag{5}$$

The 'leapfrog' scheme is one example of an unconditionally unstable scheme for the *direct* problem. It is obtained by replacing the left hand side in (3) with $\omega(u_j^n)(u_j^{n+1} - u_j^{n-1})/(2\Delta t)$. As a space marching coupled system for the IHCP this becomes:

S3   Leapfrog.

$$u_{j+1}^n = 2u_j^n + (\sigma_j^n/2)(u_j^{n+1} - u_j^{n-1}) - v_j^n - \beta_j^n(u_j^n - v_j^n)^2$$

$$v_{j+1}^n = u_j^n, \qquad n = 1, \ldots, N - 1,$$

$$u_{j+1}^N = 2u_{j+1}^{N-1} - u_{j+1}^{N-2}$$

$$v_{j+1}^N = 2v_{j+1}^{N-1} - v_{j+1}^{N-2}$$

$$u_{j+1}^0 = u_j^0, \qquad v_{j+1}^0 = v_j^0. \tag{6}$$

S1-S3 are $O(\Delta x)$ in the x-variable and lead to $u(1, t)$, $u(1 - \Delta x, t)$. The gradient at the wall can be obtained by using backward differences in x.

11

Another approach is to begin with the heat conduction equation rewritten as a space marching first order system, [3], [7], and then proceed to discretize that system. With $q = k(u)u_x$, we have

$$
\begin{aligned}
u_x &= q/k(u) \\
q_x &= \omega(u)u_t.
\end{aligned}
\tag{7}
$$

Consider first $O(\Delta x)$ schemes. The simplest example is the following:

S4   Backward.

$$
\begin{aligned}
u_{j+1}^n &= u_j^n + \Delta x\, q_j^n/k(u_j^n) \\
q_{j+1}^n &= q_j^n + \Delta x\, \omega(u_j^n)(u_j^n - u_j^{n-1})/\Delta t, \qquad n = 1, \ldots, N, \\
u_{j+1}^0 &= u_j^0, \qquad q_{j+1}^0 = q_j^0.
\end{aligned}
\tag{8}
$$

A method due to Hills and Hensel, [7], uses centered time differencing in the interior and backward time differencing at $n = N$.

S5   Hills and Hensel, (1986).

$$
\begin{aligned}
u_{j+1}^n &= u_j^n + (\sigma_j^n/2)(u_j^{n+1} - u_j^{n-1}) + \Delta x\, q_j^n/k(u_j^n) \\
q_{j+1}^n &= q_j^n + \Delta x\, \omega(u_j^n)(u_j^{n+1} - u_j^{n-1})/(2\Delta t), \qquad n = 1, \ldots, N - 1, \\
u_{j+1}^N &= u_j^N + \sigma_j^N(u_j^N - u_j^{N-1}) + \Delta x\, q_j^N/k(u_j^N) \\
q_{j+1}^N &= q_j^N + \Delta x\, \omega(u_j^N)(u_j^N - u_j^{N-1})/\Delta t \\
u_{j+1}^0 &= u_j^0 + \Delta x\, q_j^0/k(u_j^0), \qquad q_{j+1}^0 = q_j^0.
\end{aligned}
\tag{9}
$$

We now construct some further schemes based on (7).

S6   Central.

$$u_{j+1}^n = u_j^n + \Delta x\, q_j^n/(k(u_j^n))$$

$$q_{j+1}^n = q_j^n + \Delta x\, \omega(u_j^n)(u_j^{n+1} - u_j^{n-1})/(2\Delta t), \qquad n = 1,\dots,N-1,$$

$$u_{j+1}^N = 2u_{j+1}^{N-1} - u_{j+1}^{N-2}$$

$$q_{j+1}^N = 2q_{j+1}^{N-1} - q_{j+1}^{N-2}$$

$$u_{j+1}^0 = u_j^0, \qquad q_{j+1}^0 = q_j^0. \tag{10}$$

S7   Future 0.

$$u_{j+1}^n = u_j^n + \Delta x\, q_j^n/(k(u_j^n))$$

$$q_{j+1}^n = q_j^n + \Delta x\, \omega(u_j^n)(4u_j^{n+1} - u_j^{n+2} - 3u_j^n)/(2\Delta t), \quad n = 1,\dots,N-2,$$

$$u_{j+1}^{N-k} = 2u_{j+1}^{N-k-1} - u_{j+1}^{N-k-2}$$

$$q_{j+1}^{N-k} = 2q_{j+1}^{N-k-1} - q_{j+1}^{N-k-2}, \quad k = 1,0$$

$$u_{j+1}^0 = u_j^0, \qquad q_{j+1}^0 = q_j^0. \tag{11}$$

Each of **S5, S6, S7** are $O(\Delta t^2)$ schemes in the interior, with **S7** using forward time differencing. We next consider $O(\Delta t)$ forward time differencing; the forward formulae in **S9-S11** are seldom used in well-posed problems.

S8   Future 1.

$$u_{j+1}^n = u_j^n + \Delta x\, q_j^n/k(u_j^n)$$

13

$$q_{j+1}^n = q_j^n + \Delta x \; \omega(u_j^n)(u_j^{n+1} - u_j^n)/\Delta t, \qquad n = 1, \ldots, N-1,$$

$$u_{j+1}^N = 2u_{j+1}^{N-1} - u_{j+1}^{N-2}$$

$$q_{j+1}^N = 2q_{j+1}^{N-1} - q_{j+1}^{N-2}$$

$$u_{j+1}^0 = u_j^0, \qquad q_{j+1}^0 = q_j^0. \tag{12}$$

S9   Future 2.

$$u_{j+1}^n = u_j^n + \Delta x \; q_j^n / k(u_j^n)$$

$$q_{j+1}^n = q_j^n + \Delta x \; \omega(u_j^n)(u_j^{n+2} - u_j^n)/(2\Delta t), \qquad n = 1, \ldots, N-2,$$

$$u_{j+1}^{N-k} = 2u_{j+1}^{N-k-1} - u_{j+1}^{N-k-2}$$

$$q_{j+1}^{N-k} = 2q_{j+1}^{N-k-1} - q_{j+1}^{N-k-2}, \quad k = 1, 0$$

$$u_{j+1}^0 = u_j^0, \qquad q_{j+1}^0 = q_j^0. \tag{13}$$

S10   Future 3.

$$u_{j+1}^n = u_j^n + \Delta x \; q_j^n / (k(u_j^n)$$

$$q_{j+1}^n = q_j^n + \Delta x \; \omega(u_j^n)(u_j^{n+3} - u_j^n)/(3\Delta t), \qquad n = 1, \ldots, N-3,$$

$$u_{j+1}^{N-k} = 2u_{j+1}^{N-k-1} - u_{j+1}^{N-k-2}$$

$$q_{j+1}^{N-k} = 2q_{j+1}^{N-k-1} - q_{j+1}^{N-k-2}, \quad k = 2, 1, 0$$

$$u_{j+1}^0 = u_j^0, \qquad q_{j+1}^0 = q_j^0. \tag{14}$$

$$u_{j+1}^n = u_j^n + \Delta x \, q_j^n / (k(u_j^n))$$

$$q_{j+1}^n = q_j^n + \Delta x \, \omega(u_j^n)(u_j^{n+4} - u_j^n)/(4\Delta t). \qquad n = 1, \ldots, N - 4,$$

$$u_{j+1}^{N-k} = 2u_{j+1}^{N-k-1} - u_{j+1}^{N-k-2}$$

$$q_{j+1}^{N-k} = 2q_{j+1}^{N-k-1} - q_{j+1}^{N-k-2}, \quad k = 3, 2, 1, 0$$

$$u_{j+1}^0 = u_j^0, \qquad q_{j+1}^0 = q_j^0. \tag{15}$$

To construct $O(\Delta x^2)$ schemes, consider the second order Taylor expansion

$$u_{j+1}^n = u_j^n + \Delta x (u_x)_j^n + 0.5(\Delta x)^2 (u_{xx})_j^n$$

$$q_{j+1}^n = q_j^n + \Delta x (q_x)_j^n + 0.5(\Delta x)^2 (q_{xx})_j^n. \tag{16}$$

We may use (7) to express u_{xx} and q_{xx} in terms of u_t, q_t, as follows.

$$u_{xx} = q_x/k(u) - qk'(u)u_x/k^2(u)$$

$$= \omega(u)u_t/k(u) - q^2 k'(u)/k^3(u)$$

$$q_{xx} = \omega'(u)u_x u_t + \omega(u)u_{tx}$$

$$= \omega'(u)qu_t/k(u) + \omega(u)q_t/k(u) - \omega(u)k'(u)qu_t/k^2(u). \tag{17}$$

Substituting from (7) and (17), we may replace the space derivatives on the right hand side of (16) with time derivatives. Thus, with $a_j^n = \Delta x/k(u_j^n)$,

$b_j^n = 0.5(\Delta x)^2 \omega(u_j^n)/k(u_j^n)$, $c_j^n = -0.5(\Delta x)^2 k'(u_j^n)/k^3(u_j^n)$, $d_j^n = \Delta x \, \omega(u_j^n)$,

and $e_j^n = 0.5(\Delta x)^2 \left\{ \omega'(u_j^n)/k(u_j^n) - \omega(u_j^n)k'(u_j^n)/k^2(u_j^n) \right\}$, we obtain

$$u_{j+1}^n = u_j^n + a_j^n q_j^n + b_j^n (u_t)_j^n + c_j^n (q_j^n)^2$$

$$q_{j+1}^n = q_j^n + d_j^n (u_t)_j^n + b_j^n (q_t)_j^n + e_j^n q_j^n (u_t)_j^n. \qquad (18)$$

Several schemes can be constructed from (18) depending on the manner in which the time derivatives $(u_t)_j^n$ and $(q_t)_j^n$ are approximated. We define 7 such schemes, **R4** and **R6 - R11**, by stipulating that the time derivatives in (18) be approximated as in **S4** and **S6 - S11** respectively, with corresponding end-point conditions.

4   Lax-Richtmyer analysis

The Lax-Richtmyer theory of difference approximations is based on Fourier analysis of the linearized problem with constant coefficients, posed on the whole real t-line. In particular, the choice of 'boundary' approximations at $t = 0$ and $t = T_{max}$, will play no role whatever when this theory is applied to IHCP space marching schemes. Despite its shortcomings, Fourier analysis of the constant coefficient model problem is quite often a surprisingly effective diagnostic tool. Referring to equations (3) through (18) in Section 3, let $\beta_j^n = 0$, $\sigma_j^n = \sigma = (\Delta x)^2/(\Delta t \, \alpha_{min})$, $\mu = \Delta x/k_{min}$, $\gamma = \Delta x \, \omega/\Delta t$, $c_j^n = e_j^n = 0$, $a_j^n = \mu$, $b_j^n = 0.5\sigma\Delta t$, and $d_j^n = \gamma\Delta t$. Following [12, Chapters 3, 4],

16

we now view each space marching scheme as a 2×2 system

$$
\begin{aligned}
w_{j+1}(t) &= C(\Delta x, \Delta t)w_j(t), & j = 0, \dots, M-1, \\
w_0(t) &= f(t) + \delta(t), & -\infty < t < \infty.
\end{aligned}
\tag{19}
$$

Here, M is the number of space steps Δx from the interior sensor to the active surface: $C(\Delta x, \Delta t)$ is a 2×2 matrix of finite-difference operators in the t variable, assumed applied at every point : $f(t)$ denotes *exact* initial data for the IHCP such that a unique solution $u(x,t)$ exists with sufficiently many bounded derivatives: and $\delta(t)$, assumed small, represents the deviation of the actual input data from this exact data. Let $\tau_j(t)$ denote the 'truncation error' on the line $j\Delta x$, and let $\epsilon_j(t) \equiv w_j(t) - u(j\Delta x, t)$, be the difference between the exact solution of the analytic problem, and the numerical solution with noisy data. We have

$$
\begin{aligned}
\epsilon_{j+1}(t) &= C(\Delta x, \Delta t)\epsilon_j(t) + \Delta x\,\tau_j(t), \\
\epsilon_0(t) &= \delta(t).
\end{aligned}
\tag{20}
$$

Therefore,

$$
\epsilon_{j+1}(t) = C^{j+1}\,\delta(t) + \Delta x \sum_{i=0}^{j} C^{j-i}\,\tau_i(t).
\tag{21}
$$

and

$$
\| \epsilon_M \| \le \| C^M \| \,\| \delta \| + \Delta x \sum_{i=0}^{M-1} \| C^{M-1-i} \| \,\| \tau_i \| .
\tag{22}
$$

17

In (22), $\parallel \;\; \parallel$ denotes the L^2 norm in the time variable, C^M is the 'discrete solution operator', and $\parallel \tau_i \parallel = O(\Delta t + \Delta x)$, or smaller, as $\Delta t, \;\; \Delta x \downarrow 0$. Therefore, for small $\parallel \delta \parallel$, one may expect reasonable accuracy in the reconstructed surface histories, provided $\Delta t, \;\; \Delta x$ can be chosen sufficiently small without making $\parallel C^M \parallel$ too large. The latter quantity measures the amount by which noise in the interior data becomes amplified when the marching calculation reaches the active surface. We are interested in comparing the norms of discrete solution operators for the various space marching schemes *on the same mesh.*

Fourier transforming the time variable, and putting $\theta = \xi \Delta t$, where ξ is the transform variable, we may find the *amplification matrix* $G(\Delta x, \theta)$ for each of **S1-S11, R4,** and **R6-R11.** $G(\Delta x, \theta)$ is the Fourier image of $C(\Delta x, \Delta t)$, [12, p. 67], expressed in terms of the normalized frequency θ. Moreover,

$$\parallel C^M \parallel = \max_{0 \le \theta \le \pi} |G^M(\theta)|_{l^2} = A_{max}, \qquad (23)$$

where $|\;\;|_{l^2}$ denotes the Euclidean norm of G. All such matrices $G = \{g_{ij}\}$ are 2×2, and we write them in the compact notation $[g_{11}, g_{12}; g_{21}, g_{22}]$. We have:

S1 $G = [2 + \sigma - \sigma e^{-i\theta}, -1; 1, 0]$

18

S2 $\quad G = [2 - \sigma + \sigma e^{i\theta}, -1; 1, 0]$

S3 $\quad G = [2 + i\sigma sin\theta, -1; 1, 0]$

S4 $\quad G = [1, \mu; \gamma(1 - e^{-i\theta}), 1]$

S5 $\quad G = [1 + i\sigma sin\theta, \mu; i\gamma \sin\theta, 1]$

S6 $\quad G = [1, \mu; i\gamma sin\theta, 1]$

S7 $\quad G = [1, \mu; \gamma p(\theta)/2, 1] ; \quad p(\theta) = 4e^{i\theta} - e^{2i\theta} - 3$

S8 $\quad G = [1, \mu; \gamma(e^{i\theta} - 1), 1]$

S9 $\quad G = [1, \mu; \gamma(e^{2i\theta} - 1)/2, 1]$

S10 $\quad G = [1, \mu; \gamma(e^{3i\theta} - 1)/3, 1]$

S11 $\quad G = [1, \mu; \gamma(e^{4i\theta} - 1)/4, 1]$

R4 $\quad G = [1 + \sigma(1 - e^{-i\theta})/2, \mu; \gamma(1 - e^{-i\theta}), 1 + \sigma(1 - e^{-i\theta})/2]$

R6 $\quad G = [1 + i\sigma(sin\theta)/2, \mu; i\gamma sin\theta, 1 + i\sigma(sin\theta)/2]$

R7 $\quad G = [1 + \sigma p(\theta)/4, \mu; \gamma p(\theta)/2, 1 + \sigma p(\theta)/4]$

R8 $\quad G = [1 + \sigma(e^{i\theta} - 1)/2, \mu; \gamma(e^{i\theta} - 1), 1 + \sigma(e^{i\theta} - 1)/2]$

R9 $\quad G = [1 + \sigma(e^{2i\theta} - 1)/4, \mu; \gamma(e^{2i\theta} - 1)/2, 1 + \sigma(e^{2i\theta} - 1)/4]$

R10 $\quad G = [1 + \sigma(e^{3i\theta} - 1)/6, \mu; \gamma(e^{3i\theta} - 1)/3, 1 + \sigma(e^{3i\theta} - 1)/6]$

R11 $\quad G = [1 + \sigma(e^{4i\theta} - 1)/8, \mu; \gamma(e^{4i\theta} - 1)/4, 1 + \sigma(e^{4i\theta} - 1)/8]$

For the gun barrel IHCP discussed in Sections 1 and 2, we have, in previously indicated units, $\alpha_{min} = 0.004$, $\Delta t = 0.1$, and the sensor is located

19

at a distance $l = 0.5$ from the active surface $x = 1$. We place $M = 1000$ equispaced nodes on l, so that $\Delta x = 5 \times 10^{-4}$. In particular, this gives $\alpha_{min}\Delta t/(\Delta x)^2 = 1600$, so that the Courant condition for explicit time marching schemes in the direct problem, [12, p. 189], is severely violated. To complete the parameter specification, we give ω the constant value 3.2 and define $k_{min} = \omega\alpha_{min} = 0.0128$. With these parameter values, it is instructive to evaluate $|G^{1000}(\theta)|_{l^2}$ at discrete points $\theta_j = (j-1)\pi/81, \quad j = 1, 82$, for each of the above 18 schemes. This may be done easily using the software package MATLAB, [10]. The results of these computations are best described when broken up into three groups as follows:

Group I (Fig. 2A) $O(\Delta t)$ Past Temperature Schemes: **S1, S4, R4.**

Group II (Fig. 2B) $O(\Delta t^2)$ Schemes: **S3, S5, S6, S7, R6, R7.**

Group III (Fig. 2C) $O(\Delta t)$ Future Temperature Schemes: **S2, S8, S9, S10, S11, R8, R9, R10, R11.**

The Figures display $Log_{10}\{|G^{1000}(\theta)|_{l^2}\}$ versus the normalized frequency θ, on $0 \le \theta \le \pi$.

As is evident from Figs. 2A, 2B, and 2C, the maximum amplification fac-

20

tor. A_{max}, ranges from about 10^{16} in **S1**. to about 10^3 in **S11, R11**. More-over. only slight changes occur in these Figures when the number of space nodes is reduced from 1000 to 300. In particular. characteristic frequency domain signatures remain the same; Group I schemes increase monotoni-cally with θ. Group II schemes are symmetric about $\theta = \pi/2$. with a single maximum at $\pi/2$. while Group III schemes may have multiple maxima. The three schemes in Group I employ distinct space differencing methods, but share backward time differencing. In Group II. **S5, S6, R6**, have identi-cal traces; along with **S3**. these schemes use centered time differencing. but each of the four schemes uses a different space differencing technique. In Group III. **S2** results from using explicit differencing in D'Souza's method **S1**. This simple switch to forward time differencing reduces A_{max} by almost ten orders of magnitude, and renders **S2** comparable to **S5, S6, R6**. Still greater reductions are provided in **S8, R8**. by applying the same switch to **S4, R4**. The question arises as to whether substantial improvements in **S5, S6, R6**, might not result from replacing centered time differencing with a forward differencing formula that maintains $O(\Delta t^2)$ accuracy in the interior. Schemes **S7, R7**, were formulated with that purpose in mind. However. as may be seen from Fig. 2B. this particular future temperature method actually *increases* A_{max}. It is also clear from the foregoing that the

21

time differencing option plays a dominant role in determining frequency domain signatures, and that some $O(\Delta t)$ methods may be preferable to some $O(\Delta t^2)$ methods. The behavior of **S1, S2, S3**, indicates that the stability or instability of these schemes in the time marching direct problem, is of no particular relevance in the space marching inverse problem.

The remaining six schemes in Group III, **S9, R9, S10, R10, S11, R11**, are based on unconventional forms of forward differencing that induce curious frequency domain signatures, as well as substantial further reductions in A_{max}. The behavior of A_{max} can be correlated with the non dimensional parameter $\Omega = l(\alpha_{min}\Delta t)^{-1/2}$ mentioned in the Introduction. We have $\Omega = 25$ in Figs. 2A, 2B, and 2C. In Fig. 3A, Group I schemes are reexamined with $l = 1.0$ and all other parameter values unchanged, so that $\Omega = 50$. In Fig. 3B, Group II schemes are reevaluated with $\Delta t = 0.01$ and all other parameters as in Fig. 2B, so that $\Omega = 79$. Finally, in Fig. 3C, Group III schemes are considered with $\Omega = 250$, resulting from using $\Delta t = 0.01$, $\alpha_{min} = 0.0004$, $k_{min} = 0.00128$, and the remaining parameters as in Fig. 2C. Together with further computations involving various combinations of parameters and a fair range of Ω values, these Figures indicate an asymptotic rule of thumb, $A_{max} \approx 10^{\lambda\Omega}$, where λ is a slowly varying function of the parameters that may be taken as a constant. Thus, $\lambda \approx 0.6$

in Group I schemes. In Group II, $\lambda \approx 0.3$ for **S5, S6, R6**, while $\lambda \approx 0.35$ for **S7, R7**. In Group III, $\lambda \approx 0.12$ for **S11, R11**, gradually increasing to about twice that value for **S8, R8**. In Groups II and III, the **R** schemes, which are second order accurate in the space variable, are better behaved than their **S** counterparts. In summary, the best schemes in Group II blow-up like the square root of **S1**, while the best schemes in Group III blow-up like the fifth root of **S1**.

5 A numerical experiment

It remains to demonstrate the relevance of the preceding analysis in the computation of the nonlinear IHCP, on a finite t-interval, with end-point conditions. With reference to Fig. 1 in Section 2, we seek to recover rapid temperature and flux pulses at $x = 1$, from highly attenuated interior data. Consider first the easier problem of reconstruction from $x = 0.7$ when no random noise is added to the data. In this case $\Omega = 15$. The slight amount of residual data noise originating from numerical computation of the direct problem, is nevertheless sufficient to trigger instabilities if Group I schemes are used. On the other hand, Group II and III schemes perform well under these conditions. For example, as shown in Fig. 4, **S5, S6, S7, S8,**

reproduce the exact temperature and gradient histories. An irksome side effect of Group III schemes with multiple maxima is an *overdamping* of certain frequency ranges, which causes **S9, S10, S11**, to *underestimate* the true solutions. This effect is more pronounced in the case of the narrow flux pulse, than in the case of the temperature pulse. For the temperature history, the true maximum is underestimated by 0.7% with **S9**, 1.1% with **S10**, and 1.4% with **S11**. The corresponding peak gradient underestimates are 3.6%, 5.3%, and 6.8%, respectively. The worst case, **S11**, is shown in Fig. 5. Note that the last five milliseconds of each trace in Figs. 4 and 5 have been deleted; this is the region where the reconstruction is seriously affected by end-point instabilities.

The situation changes drastically when we attempt reconstruction from $x = 0.5$ with 0.1% random noise added to the interior data. Now, with $\Omega = 25$, all Group I and Group II schemes are hopelessly unstable. The behavior of **S6**, shown in Fig. 6, is typical of Group II schemes and leads to amplitudes on the order of 10^6. In addition, most Group III schemes fail to produce recognizable traces in this representative, yet difficult, inverse computation. However, useful information is recoverable with either of **S11**, **R11**, as may be seen in Fig. 7. Although badly contaminated by noise and unable to match the true maximum, the reconstructed gradient provides

24

a fair representation of the concentrated flux waveform at $x = 1$. The slower temperature pulse emerges relatively well. The result of post-filtering the preceding computation in the time domain, using a three term moving average, is shown in Fig. 8. If the level of noise in the interior data is increased to 1%, **S11, R11** fail to produce satisfactory results, even after smoothing. On the other hand, with 0.01% added noise, **S9, R9** provide reconstructions of somewhat better quality than in Figs. 7 and 8, and with better estimates of the true maxima.

We have not discussed *regularization* of the IHCP in the present paper. For the linear problem with constant coefficients, [3], or, more generally, whenever the analytic solution operator for the direct problem is *known*, Tikhonov regularization techniques may be applied to control the growth of errors. In the case analyzed in [3], such regularization is shown to be equivalent to subjecting the initial data to a specific low-pass filter in the Fourier transform domain. One may also apply the appropriate fractional power of that filter at every step of a space marching calculation. For nonlinear problems, stepwise filtering based on the related linearized problem at each step can sometimes be useful, [4]. However, regularization techniques in marching computations are likely to be effective only if the underlying difference scheme blows-up relatively slowly with Ω. The design of such regularized

marching algorithms is another motivation for the present study.

References

[1] J. V. Beck, B. Blackwell, and C.R. St. Clair, Jr., *Inverse Heat Conduction*, Wiley-Interscience, New York, 1985.

[2] T. L. Brosseau, B. B. Grollman, and J. R. Ward, *Prediction of erosion from heat transfer measurements*, ARBRL-TR-02181, (July 1979), Ballistic Research Laboratory, Aberdeen Proving Ground, MD. Available from National Technical Information Service, U.S. DoC, Springfield, VA. 22161.

[3] A. Carasso, *Determining surface temperatures from interior observations*, SIAM J. Appl. Math., 42, (1982), pp. 558-574.

[4] A. S. Carasso, *Nonlinear inverse heat transfer calculations in gun barrels*, Transactions of the First Army Conference on Applied Mathematics and Computing, George Washington University, Washington, D. C., May 9-11, 1983. U. S. Army Research Office, Report No. 84-1, Research Triangle Park, NC, 1984, pp. 325-353.

[5] L. Eldén, *Approximations for a Cauchy problem for the heat equation*, Inverse Problems, 3, (1987), pp. 263-273.

[6] D. N. Hào and R. Gorenflo, *A non-characteristic Cauchy problem for the heat equation*, Report No A-90-12, (1990), Institute for Mathematics, Free University-Berlin, Germany.

[7] R. G. Hills and E. C. Hensel, Jr., *One dimensional nonlinear inverse heat conduction technique*, Numerical Heat Transfer, 10, (1986), pp. 369-393.

[8] N. K. Madsen and R. F. Sincovec, *PDECOL, General collocation software for partial differential equations*, ACM Transactions on Mathematical Software, 5, (1979), pp. 326-351.

[9] W. Marquardt and H. Auracher, *An observer-based solution of inverse heat conduction problems*, Int. J. Heat Mass Transfer, 33, (1990), pp. 1545-1562.

[10] ———,*PRO-MATLAB User's Guide*, The Mathworks, Inc., 21 Eliot Street, South Natick, MA, 01760.

[11] M. Raynaud and J. Bransier, *A new finite difference method for the nonlinear inverse heat conduction problem*, Numerical Heat Transfer, 9, (1986), pp. 27-42.

[12] R. D. Richtmyer and K. W. Morton, *Difference Methods for Initial Value Problems*, 2nd ed., Wiley-Interscience, New York, 1967.

[13] ————,*1990 Steele Prizes*, Notices of the American Mathematical Society, 37, (1990), pp. 801- 807.

[14] J. W. Spretnak and Cyril Wells, *An engineering analysis of the problem of quench cracking in steel*, Transactions of the American Society for Metals, 42, (1950), pp. 233-269.

[15] Y. S. Touloukian, Ed., *Thermophysical Properties of High Temperature Solid Materials, Volume 3: Ferrous Alloys*, Macmillan, New York, 1967.

[16] J. R. Ward and T. L. Brosseau, *Effect of wear reducing additives on heat transfer into the 155 mm M185 cannon*, BRL-MR 2730, (February 1977), Ballistic Research Laboratory, Aberdeen Proving Ground, MD. Available from National Technical Information Service, U.S. DoC, Springfield, VA, 22161.

[17] C. F. Weber. *Analysis and solution of the ill-posed inverse heat conduction problem*, Int. J. Heat Mass Transfer, 24, (1981), pp. 1783-1792.
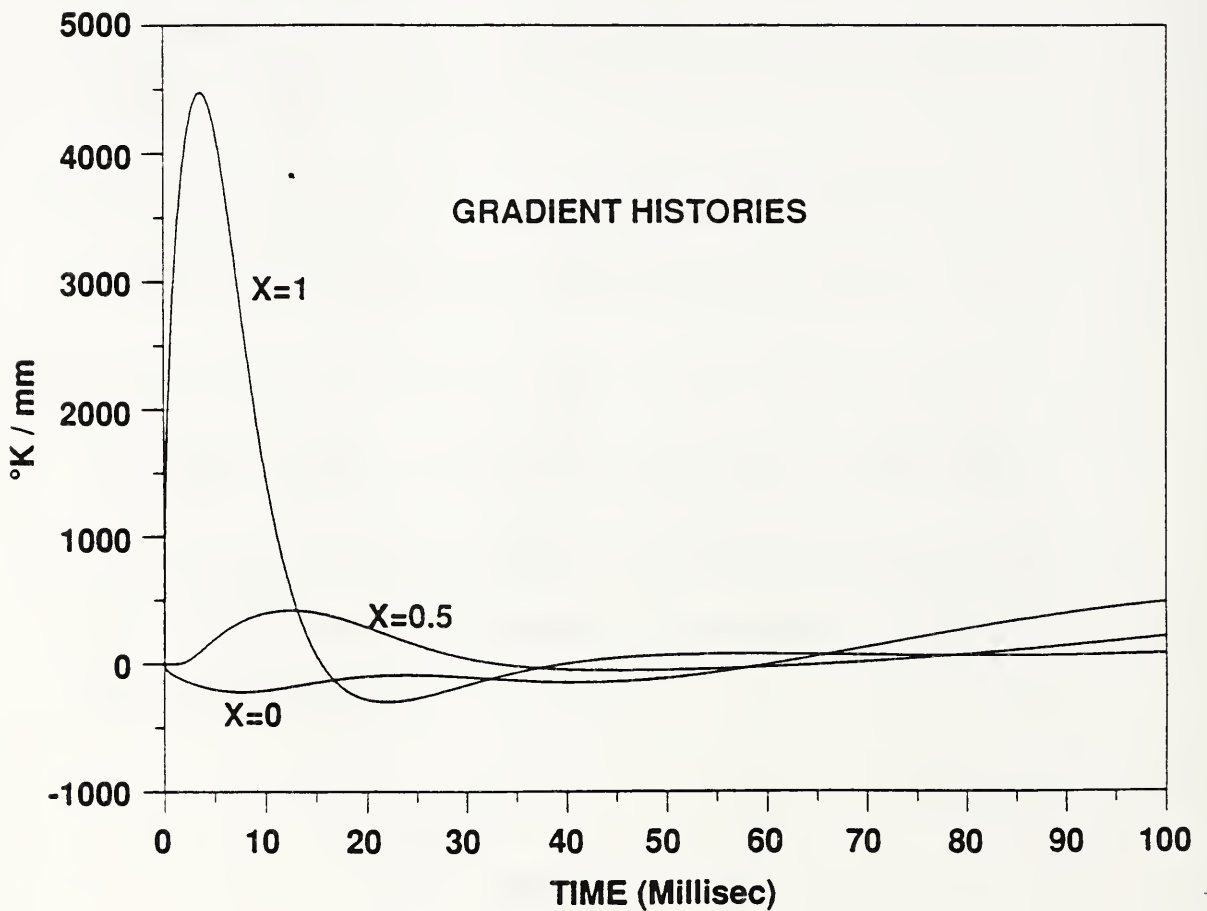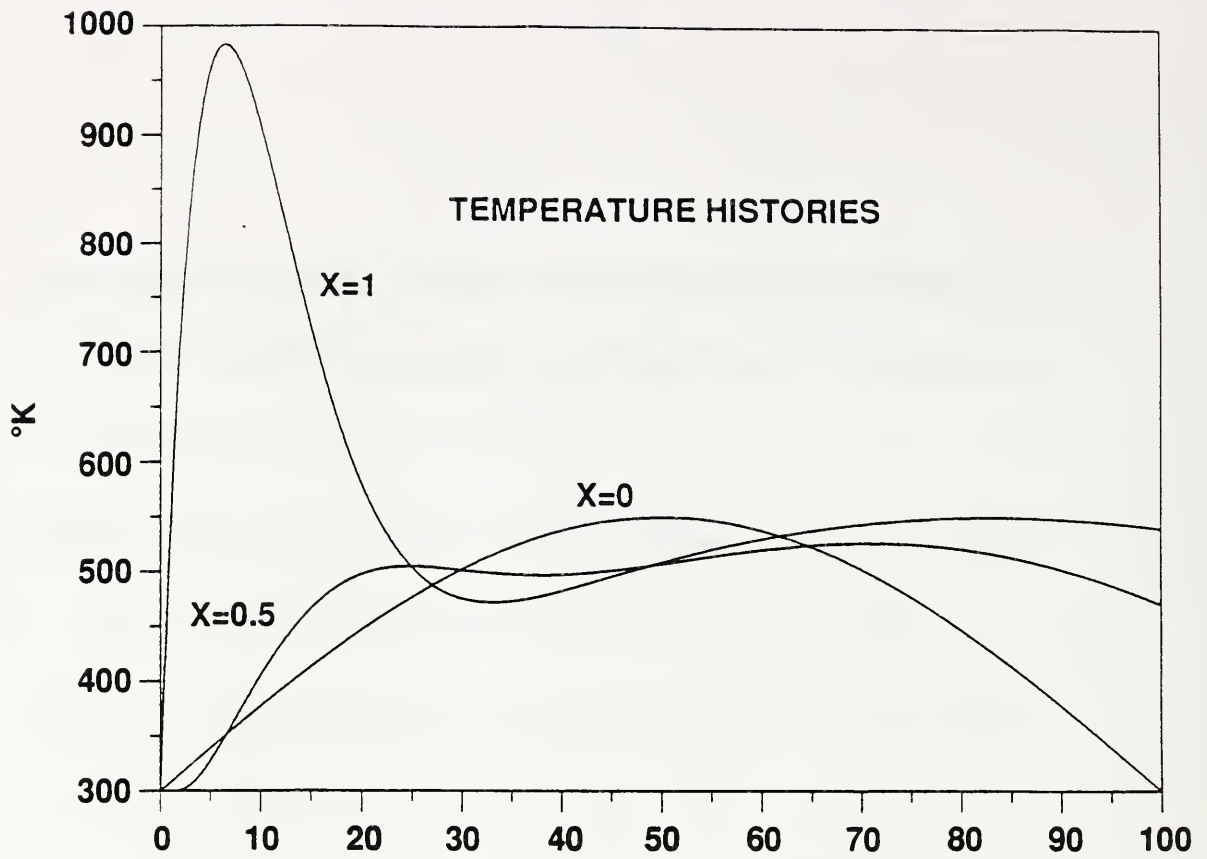
Figure 1
Exact solution of the direct problem at $x = 0$, 0.5, 1.0.
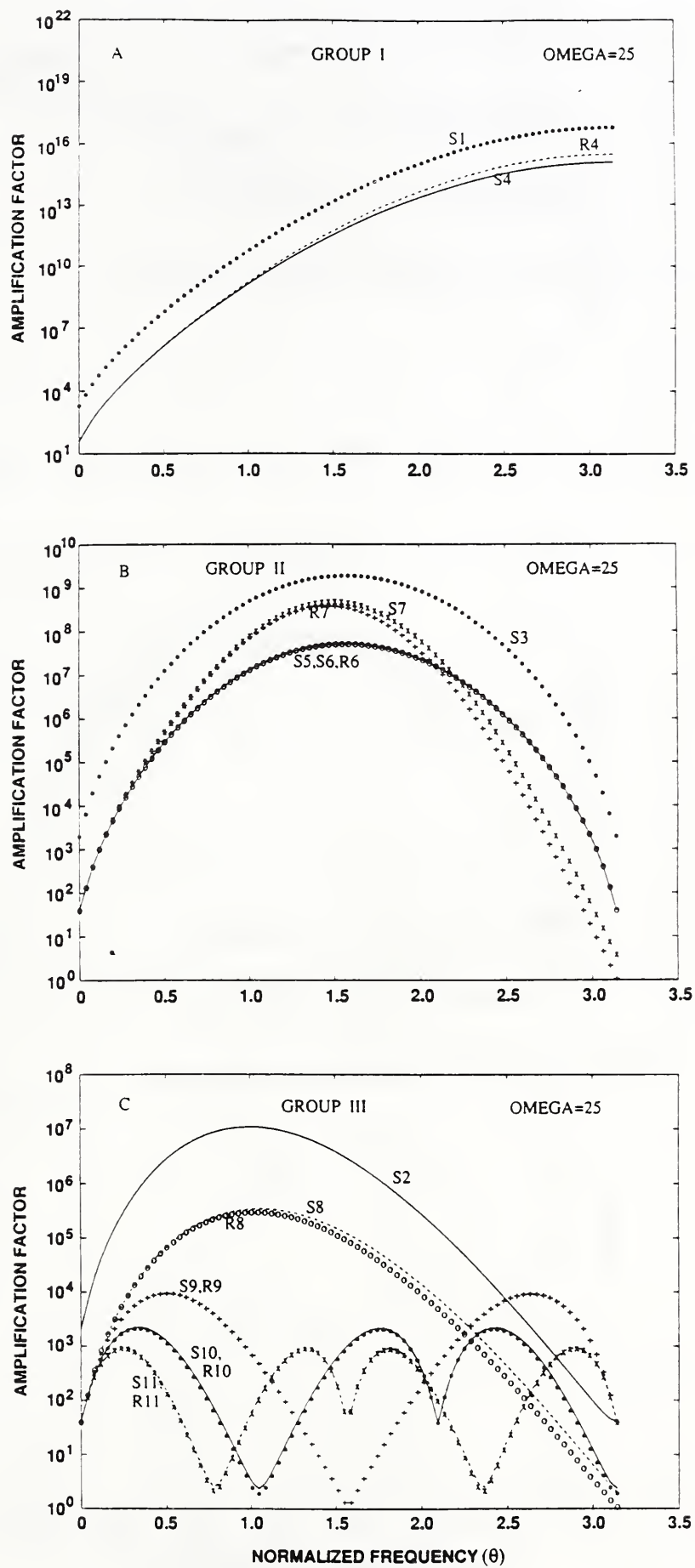
Figure 2

Behavior of $|G^{1000}(\theta)|_{l^2}$ on the mesh $\Delta t = 0.1$, $\Delta x = 5 \times 10^{-4}$.

31
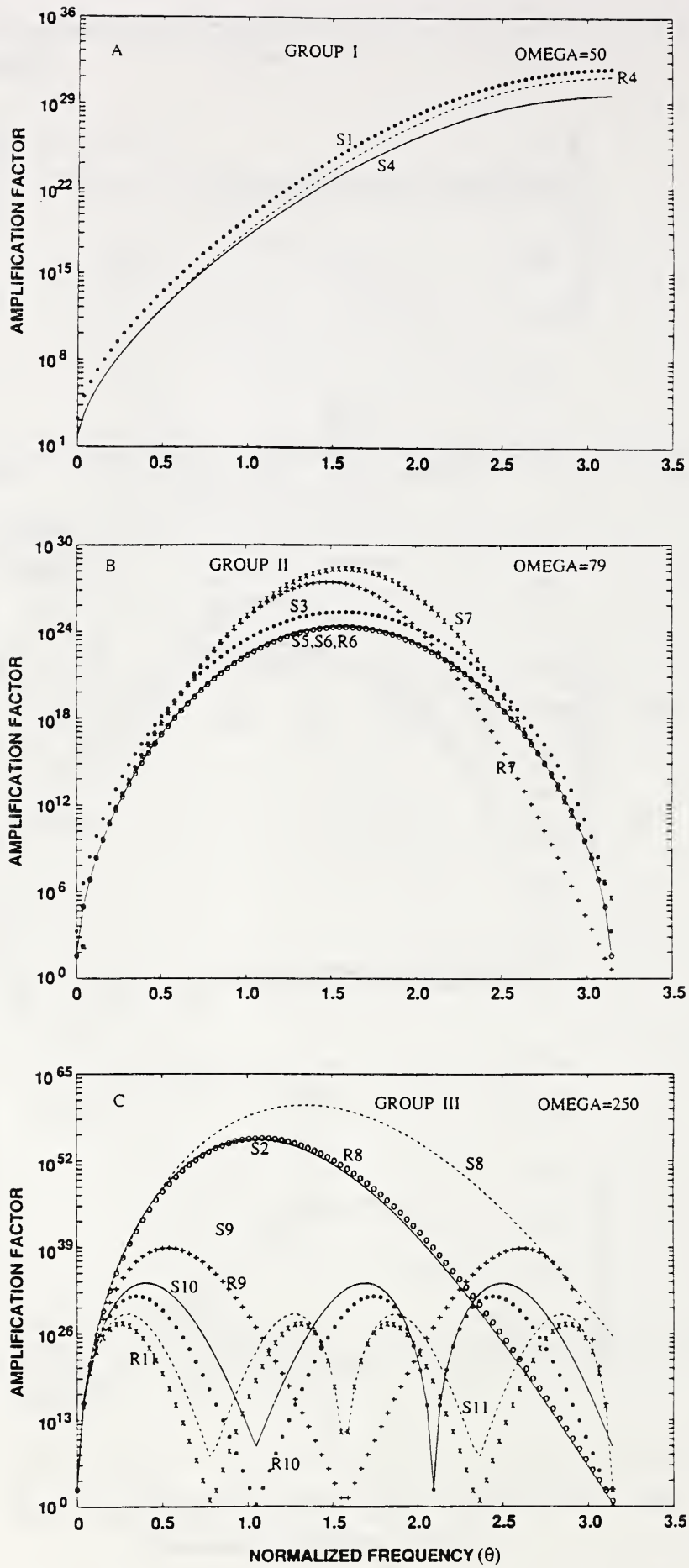
Figure 3

Behavior of $|G^{1000}(\theta)|_{l^2}$ at various values of Ω.
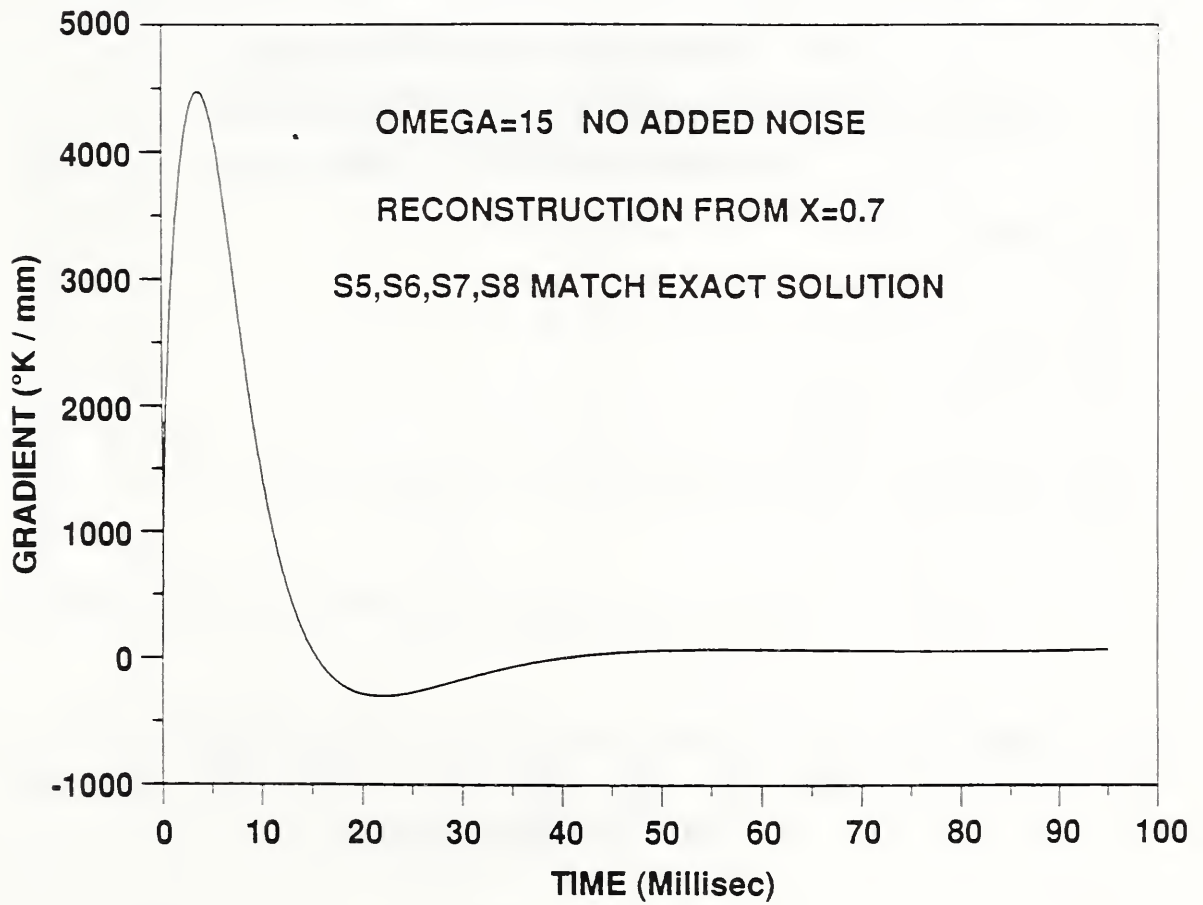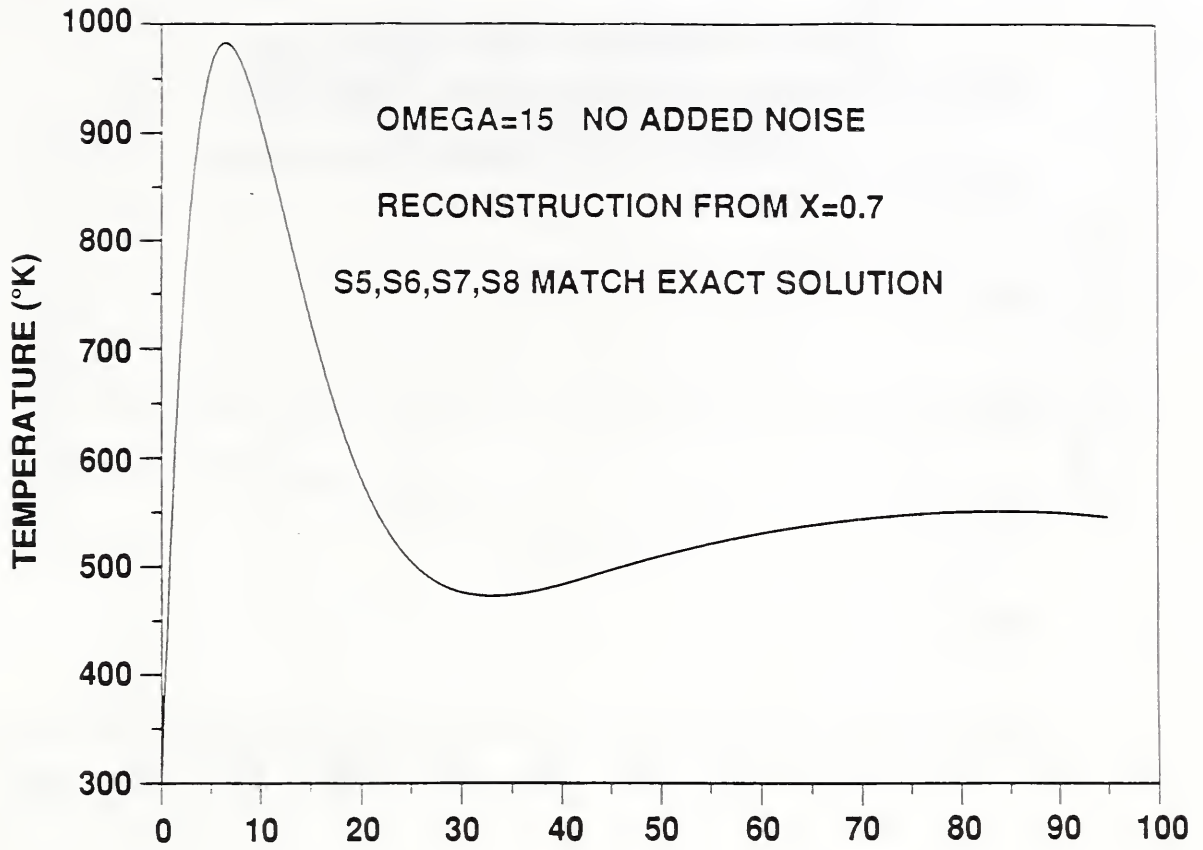
Figure 4
Nonlinear reconstruction under favorable conditions.
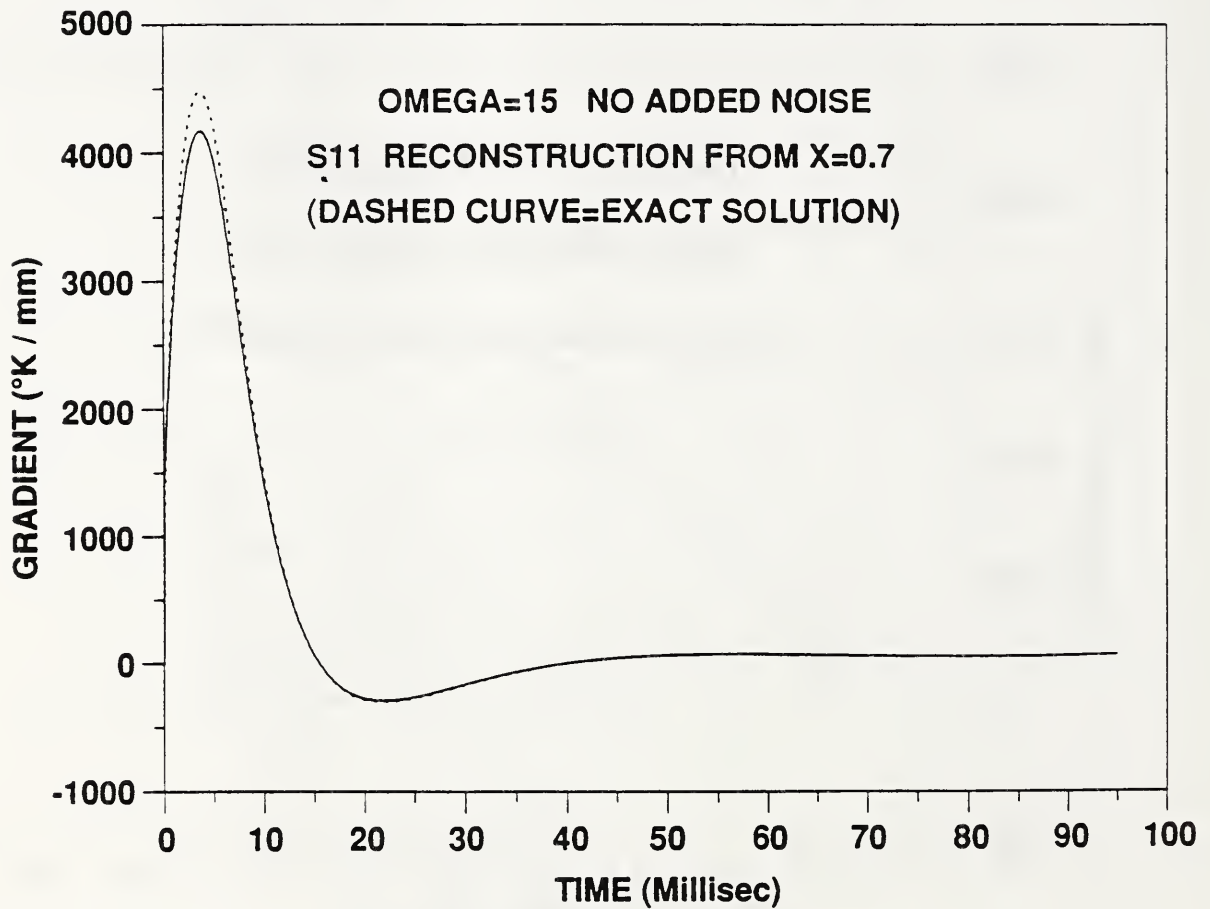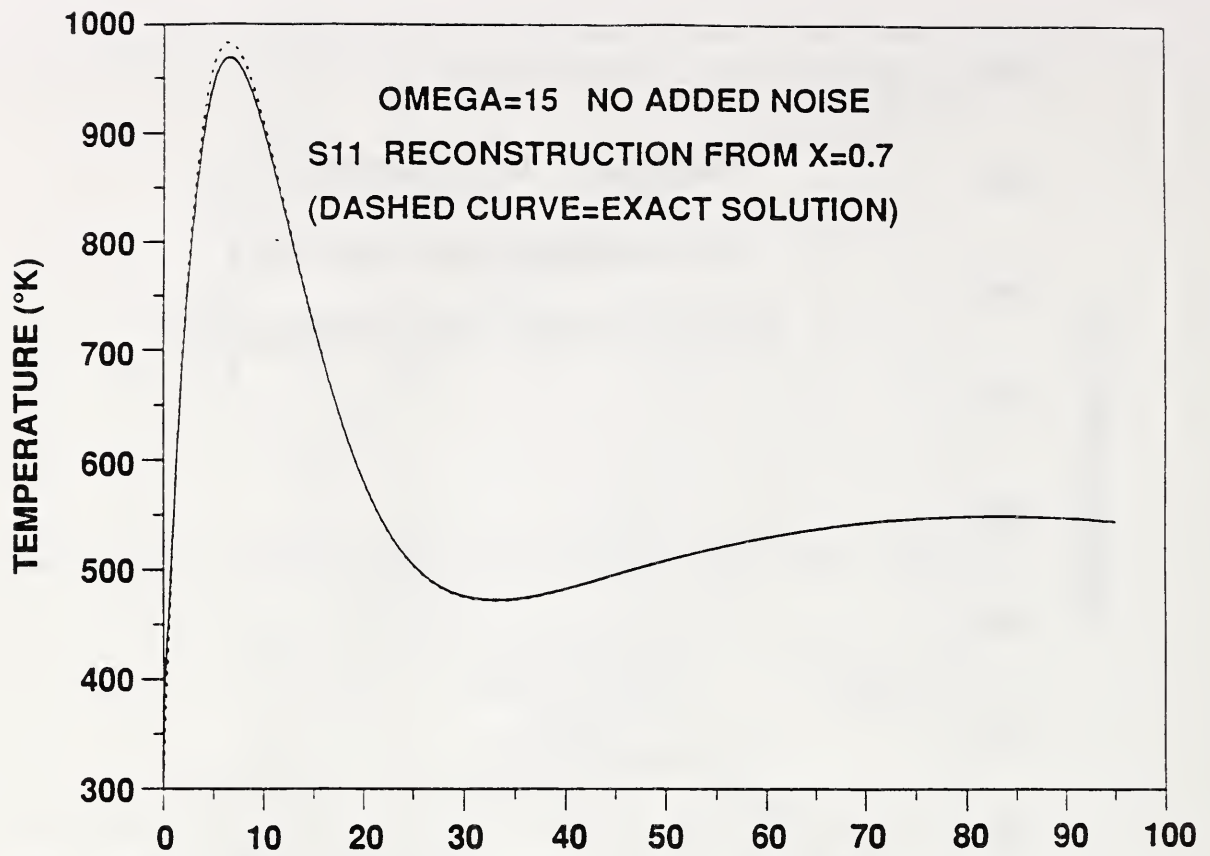
Figure 5

Overdamping in S11 leads to 1.4% (6.8%) underestimate of peak temperature (gradient) in reconstruction from $x = 0.7$.
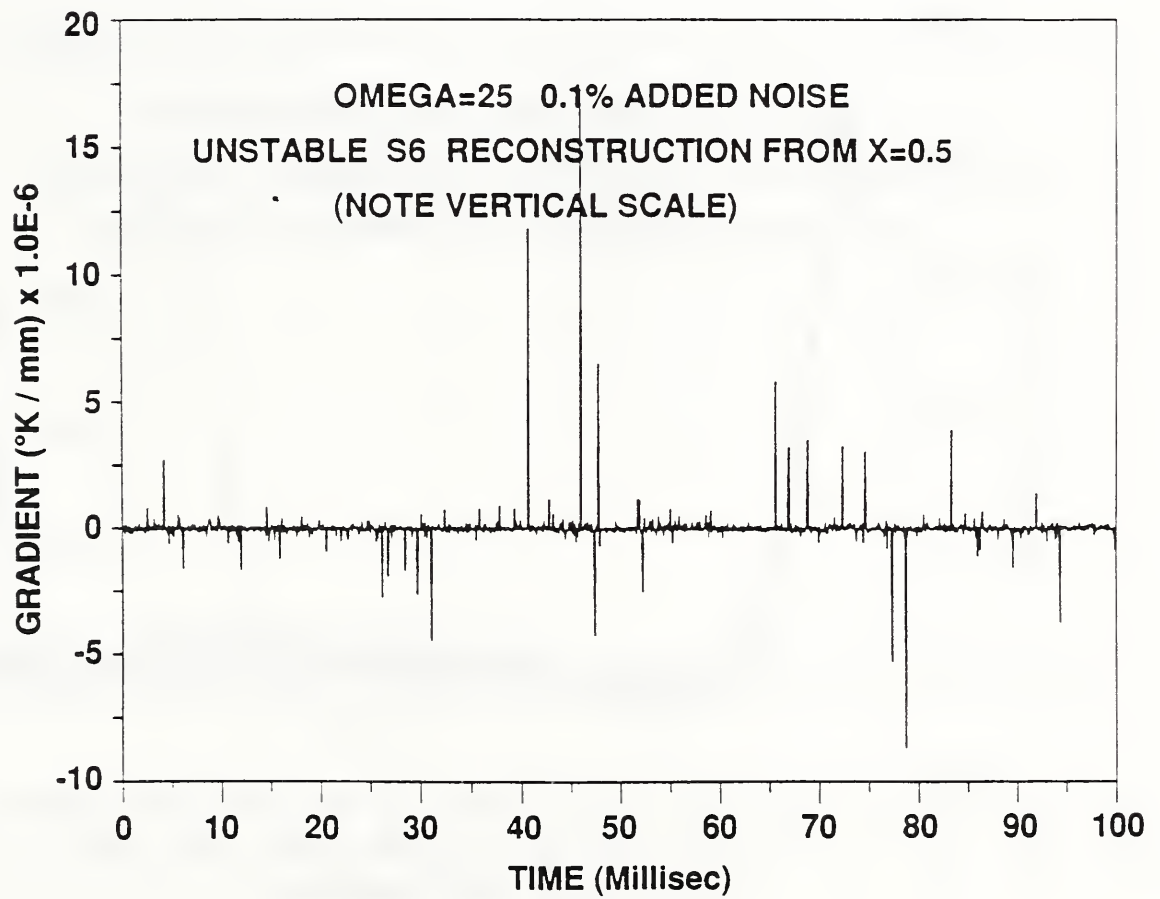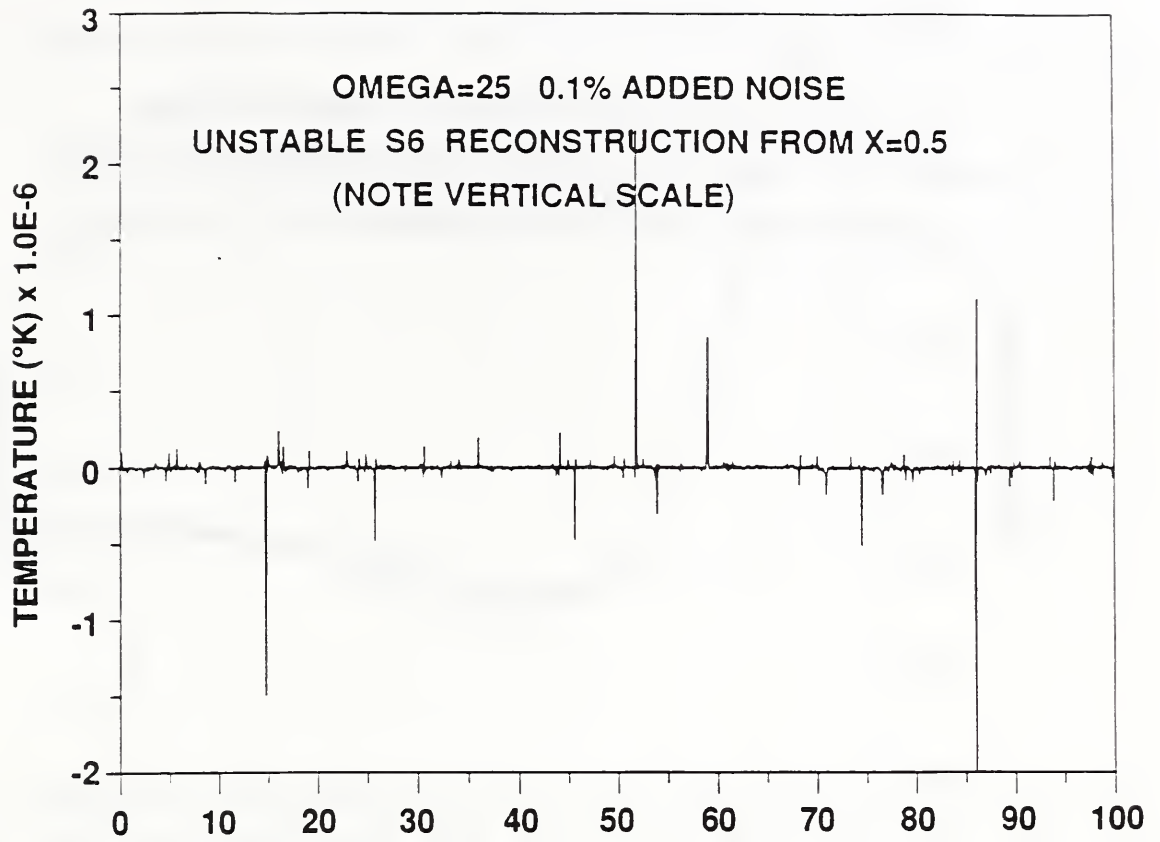
Figure 6

Behavior of S6 under adverse conditions is typical of Group II schemes.
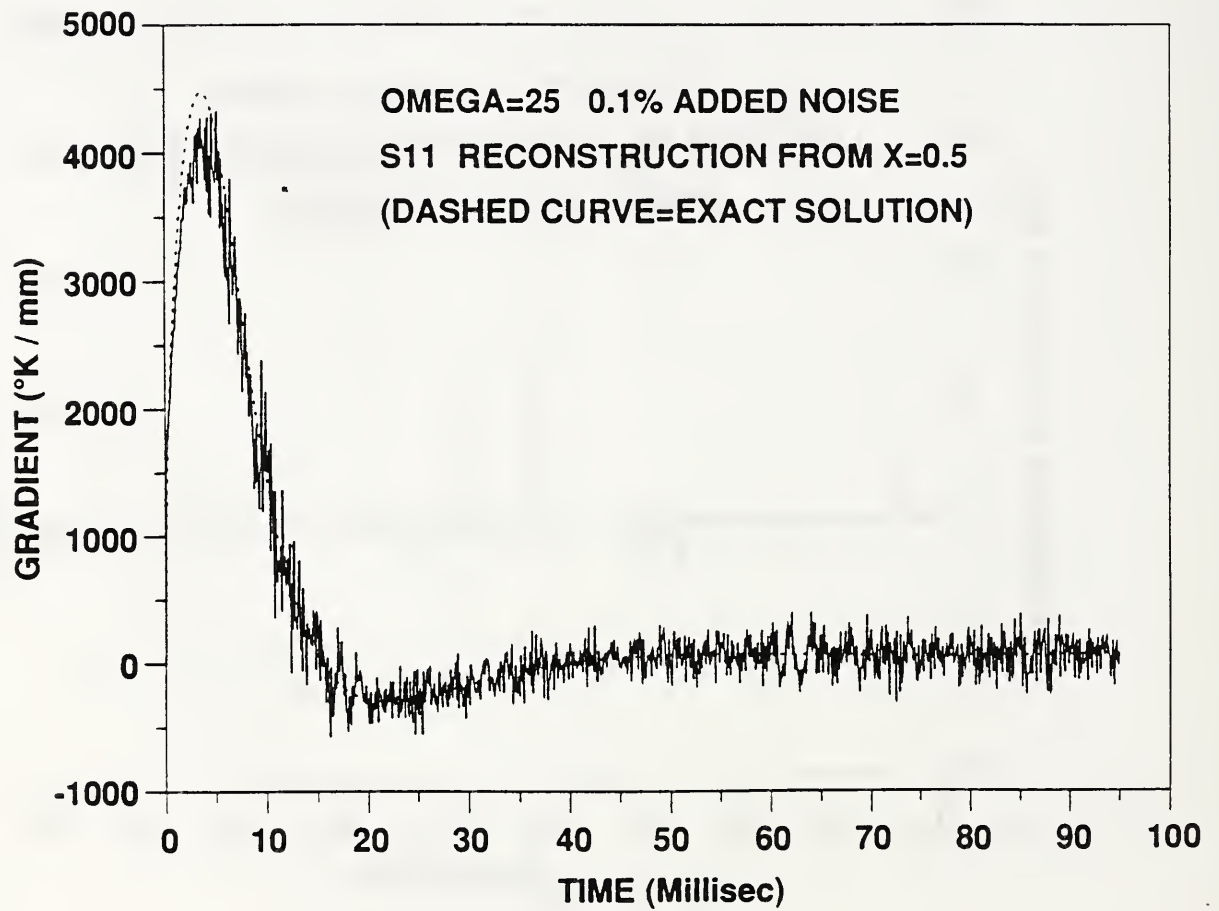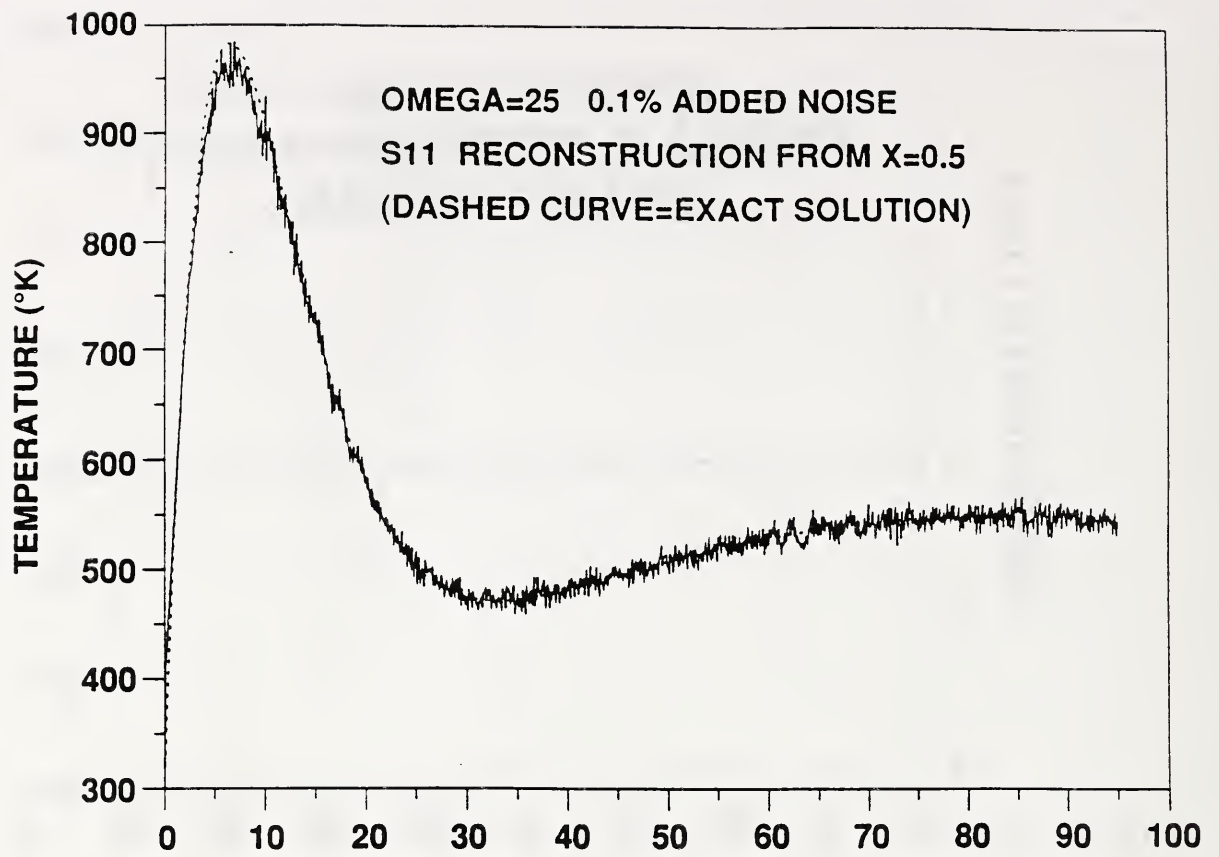
Figure 7
Unsmoothed S11 reconstruction.
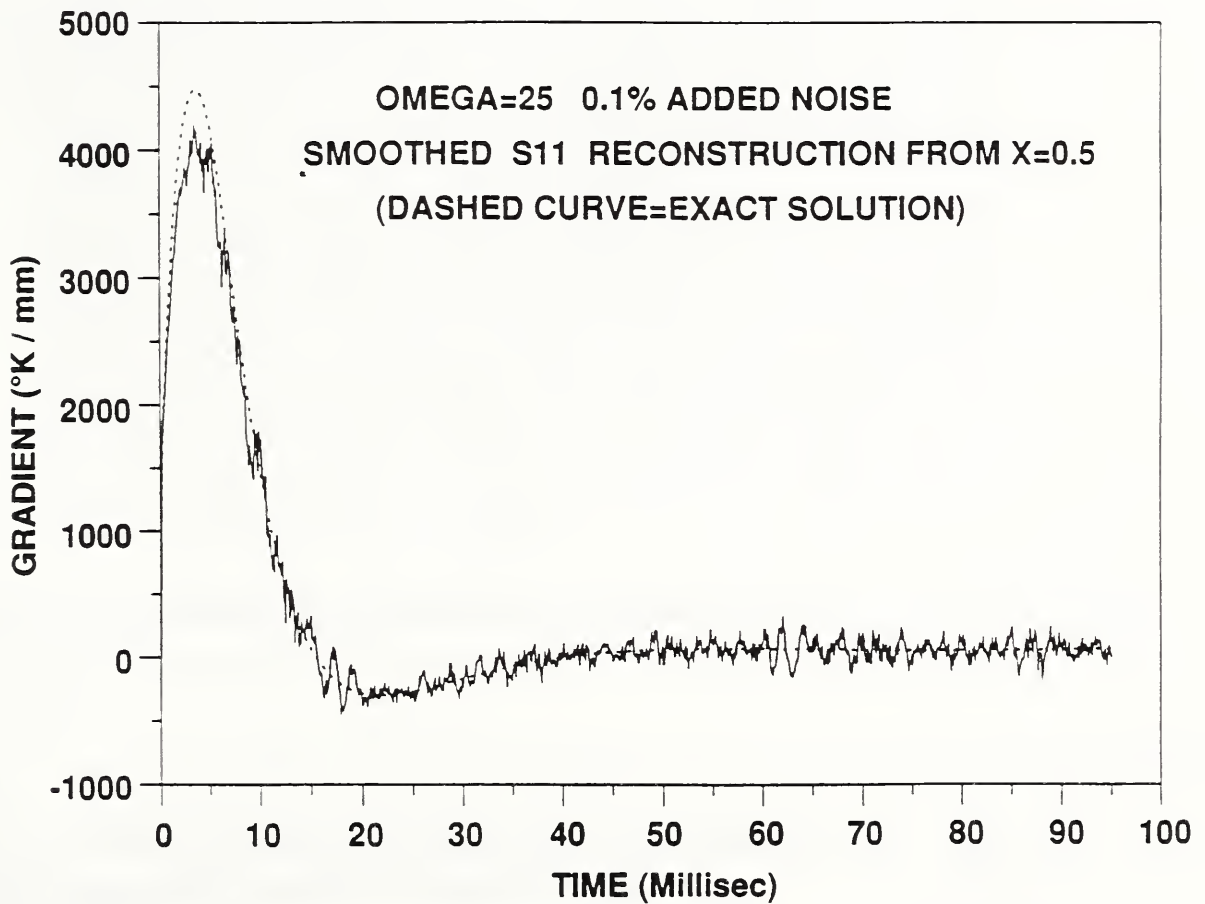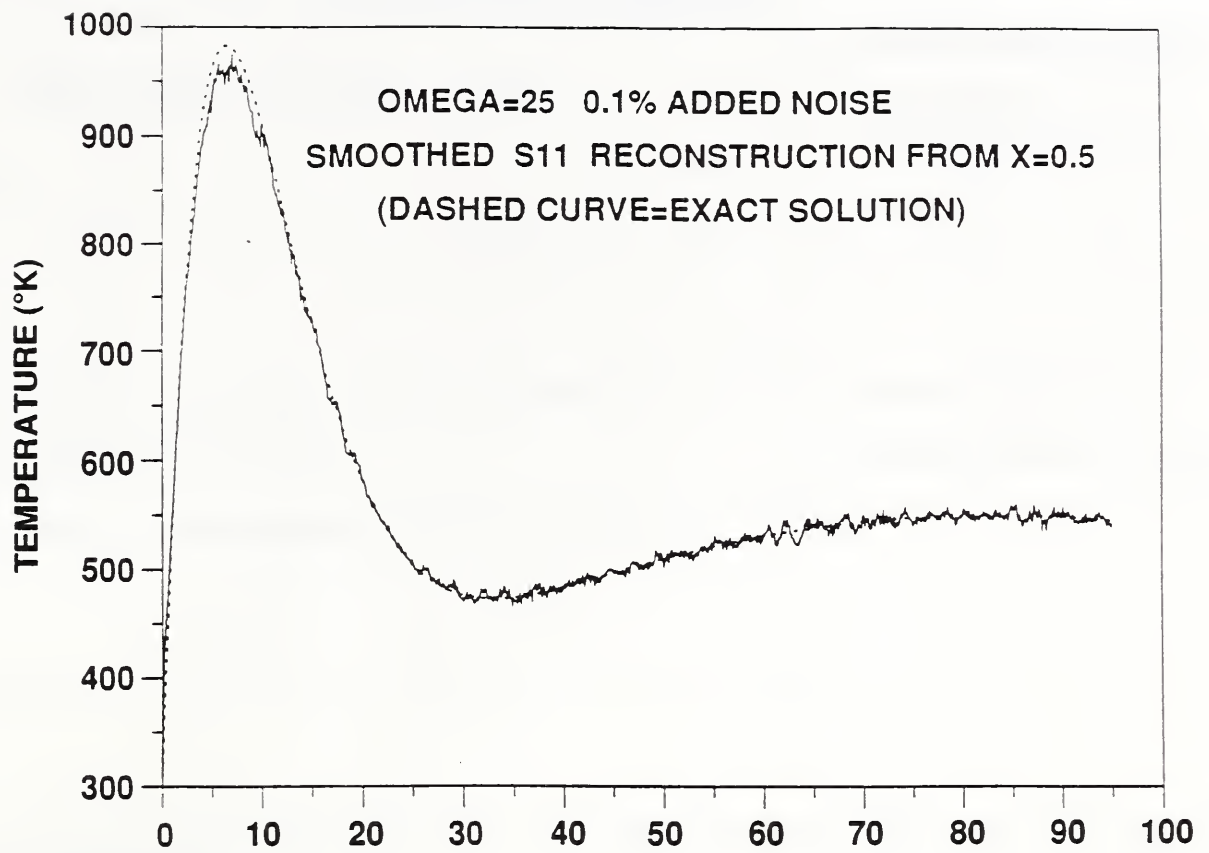
Figure 8

Smoothed S11 reconstruction using three term moving average.

4. TITLE AND SUBTITLE

Space Marching Difference Schemes in the Nonlinear Inverse Heat Conduction Problem

5. AUTHOR(S)

Alfred S. Carasso

11. ABSTRACT (A 200-WORD OR LESS FACTUAL SUMMARY OF MOST SIGNIFICANT INFORMATION. IF DOCUMENT INCLUDES A SIGNIFICANT BIBLIOGRAPHY OR LITERATURE SURVEY, MENTION IT HERE.)

The Lax-Richtmyer theory is used to study the error amplification properties of 18 space marching finite difference schemes, for the 1-D nonlinear inverse heat conduction problem. A non-dimensional parameter Ω, involving the time step Δt, the effective thermal diffusivity α, and the distance l from the sensor to the active surface, provides a measure of the numerical difficulty of the inverse calculation. All 18 schemes are unstable and blow-up like $10^{\lambda\Omega}$, where the constant λ depends on the particular numerical method. However, there are substantial differences in the $\lambda's$, and some newly constructed algorithms, employing forward time differences at non-adjacent mesh points, are shown to produce relatively low values of λ. Using synthetic noisy data, a nonlinear reconstruction problem is considered for which $\Omega = 25$. This problem simulates heat transfer in gun barrels when a shell is fired. It is shown that while most of the 18 schemes cannot recover the thermal pulses at the gun tube wall, two of the new methods provide reasonably accurate results. A tendency to underestimate peak values in fast, narrow thermal pulses, is also noted.

12. KEY WORDS (6 TO 12 ENTRIES; ALPHABETICAL ORDER; CAPITALIZE ONLY PROPER NAMES; AND SEPARATE KEY WORDS BY SEMICOLONS)

Error amplification; gun barrels; inverse heat conduction; Lax-Richtmyer theory; space marching schemes

IR 4483

UNAVAILABLE FOR BINDING